Photoluminescence and Magnetism in the New Magnetic Semiconductors: $K_2Cd_{3(1-x)}Mn_{3x}S_4$

Enos A. Axtell, III,[†] Jason Hanko,[†] Jerry A. Cowen,[‡,§] and Mercouri G. Kanatzidis*,[†]

Departments of Chemistry and Physics and Astronomy, and Center for Fundamental Materials Research, Michigan State University, East Lansing, Michigan 48824-1322

Received January 18, 2001. Revised Manuscript Received May 22, 2001

A new family of magnetic semiconductors, $K_2Cd_{3(1-x)}Mn_{3x}S_4$, prepared from molten K_2S_x is reported. For $x \leq 0.6$, the compounds crystallize in the $K_2Cd_3S_4$ structure type. The cell volumes of the series obey Vegard's Law for solid solutions. The compounds range in color from yellow through orange brown to red and possess platelike morphologies. A structural transformation occurs between $x = 0.7$ and $x = 0.9$. Red plates of $K_2Cd_{0.4}Mn_{2.6}S_4$ ($x = 0.87$) crystallize in the space group *Ccca* with $a = 5.9217(8)$ Å, $b = 13.531(1)$ Å, $c = 11.0696(8)$ Å, and $V = 887.0(1)$ Å^3. The end member, $K_2Mn_3S_4$, crystallizes in the space group *Ccca* with $a = 11.0637(7)$ Å, $b = 26.830(2)$ Å $c = 5.8180(4)$ Å, and $V = 1727$ Å^3. For $x \leq 0.6$, the compounds form as $(M_3S_4)_n^{2n-}$ layers, interspersed by K^+ cations. These layers are composed only of $M_3S_4^{2-}$ units shaped like truncated cubes. When $x = 0.87$, a new structure related to that of $Cs_2Mn_3S_4$ is observed. The end member of the series (i.e., $x = 1$) $K_2Mn_3S_4$ is revealed to have a related yet surprising structure. The compounds display room-temperature band gaps ranging from 2.79 to 2.92 eV. Absorptions in the mid-gap region, due to Mn^{2+}-based d−d transitions, are also observed. The compounds are strongly emissive in the visible spectrum at room temperature, with the light emission shifted to the red immediately upon the introduction of small amounts of manganese. The magnetic properties of these compounds evolve from classical paramagnetic to spin glass as a function of x. For $x \geq 0.05$, the compounds deviate from Curie−Weiss behavior. Antiferromagnetic coupling is observed in all cases. With very high Mn content transitions to magnetically complex phases are observed with possible spin-glass-like behavior.

Introduction

Compounds that display both semiconducting and magnetic properties are interesting experimentally, theoretically, and technologically.[1] Over the last several decades, interest has focused on the so-called II−VI compounds of the type $M_{1-x}Mn_xQ$ (M = Zn, Cd, Hg; Q = S, Se, Te).[2] These dense, three-dimensional compounds display tetrahedral coordination about both the metal and the nonmetal and their crystallographic, optical, and magnetic properties have been studied thoroughly. Another facet of magnetic semiconductor research is the study of manganese-doped, II−VI quantum-sized particles as for example the $Cd_{1-x}Mn_xSe$ system.[3,4] The particles display increasing band gaps with increasing manganese content, and spin glass behavior is observed for low concentrations of Mn.[5] Other dilute magnetic semiconductor systems with interesting magnetic properties include $Zn_{2-x}Mn_xP_2S_6$[6] and $Cd_{2-x}Fe_xP_2S_6$[7] and $Zn_{1-x}Mn_xGa_2Se_4$[8] with $0 < x <$

* To whom correspondence should be addressed.
[†] Department of Chemistry.
[‡] Department of Physics and Astronomy.
[§] Deceased.

(1) Ohno, H.; Chiba, D.; Matsukura, F.; Omiya, T.; Abe, E.; Dietl, T.; Ohno, Y.; Ohtani, K. *Nature* **2000**, *408*, 944−946. (b) Ohno, H. *Science* **1998**, *281*, 951−956. (c) Twardowski, A. *Mater. Sci. Eng., B* **1999**, *63*, 96−102. (d) Bourgognon, C.; Tatarenko, S.; Cibert, J.; Gilles, B.; Marty, A.; Samson, Y. *Appl. Phys. Lett.* **1999**, *75*, 2818−2820. (e) Dietl, T.; Ohno, H.; Matsukura, F.; Cibert, J.; Ferrand, D. *Science* **2000**, *287*, 1019−1022. (f) Lidiard, A. B. *Rep. Prog. Phys.* **1954**, *27*, 201.

(2) *Diluted Magnetic (Semimagnetic) Semiconductors*; Aggarwal, R. L., Furdyna, J. K., von Molnar, S., Eds.; Materials Research Society Symposia Proceedings; Materials Research Society: Pittsburgh, PA, 1987; Vol. 89, and references therein. (b) Bindilatti, V.; ter Haar, E.; Oliveira, N. F.; Shapira, Y.; Liu, M. T. *Phys. Rev. Lett.* **1998**, *80*, 5425−5428. (c) Levy, L.; Ingert, D.; Feltin, N.; Pileni, M. P. *Adv. Mater.* **1998**, *10*, 53. (d) Lunn, B.; Davies, J. J. *Semicond. Sci. Technol.* **1990**, *5*, 1155−1160.

(3) Kim, K. W. Ph.D. Dissertation, Michigan State University, East Lansing, MI, 1993. (b) Kim, K.-W.; Cowen, J. A.; Dhingra, S.; Kanatzidis, M. G. In *Chemical Processes in Inorganic Materials: Metal and Semiconductor Clusters and Colloids*; Bradley, J. S., Persans, P. D., Schmid, G., Chianelli, R. R., Eds.; Materials Research Society Symposia Proceedings; Materials Research Society: Pittsburgh, PA, 1992; Vol. 272, pp 27−33. (b) Levy, L.; Feltin, N.; Ingert, D.; Pileni, M. P. *Langmuir* **1999**, *15*, 3386−3389. (c) Feltin, N.; Levy, L.; Ingert, D.; Pileni, M. P. *J. Phys. Chem. B* **1999**, *103*, 4−1. (d) Pileni, M. P. *Cryst. Res. Technol.* **1998**, *33*, 1155−1186.

(4) Levy, L.; Ingert, D.; Feltin, N.; Pileni, M.-P. *Adv. Mater.* **1998**, *10*, 53.

(5) Yang, Y. Q.; Keesom, P. H.; Furdyna, J. K.; Giriat, W. *J. Solid State Chem.* **1983**, *49*, 20−24. (b) Twardowski, A.; Denissen, C. J. M.; Dejonge, W. J. M.; Dewaele, A.; Demianiuk, M.; Triboulet, R. *Solid State Commun.* **1986**, *59*, 199−203. (c) Bandaranayake, R. J.; Lin, J. Y.; Jiang, H. X.; Sorensen, C. M. *J. Magn. Magn. Mater.* **1997**, *169* (3), 289−302. (d) Bandaranayake, R. J.; Smith, M.; Lin, J. Y.; Nang, H. X.; Sorensen, C. M. *IEEE Trans. Magn.* **1994**, *30*, 4930−4932.

(6) Chandrasekharan, N.; Vasudevan, S. *Phys. Rev. B−Condens. Matter Mater. Phys.* **1996**, *54*, 14903−14906. (b) Goossens, D. J.; Hicks, T. J. *J. Phys.: Condens. Matter* **1998**, *10*, 7643−7652.

(7) Leaustic, A.; Riviere, E.; Clement, R.; Manova, E.; Mitov, I. *J. Phys. Chem. B* **1999**, *103*, 4833−4838.

(8) Moron, M. C.; Campo, J.; Palacio, F.; Attolini, G.; Pelosi, C. *J. Magn. Magn. Mater.* **1999**, *197*, 437−439.

10.1021/cm0100422 CCC: $20.00
Published on Web 08/24/2001

1. Antiferromagnetic- as well as spin-glass-like behavior was observed depending on the Mn content and the cation distribution. Dilute magnetic semiconductor systems are now attracting considerable interest for their potential in the field of spintronics where electrically controlled ferromagnetism in manganese compound semiconductors opens prospects for tailoring magnetic- and spin-related phenomena in semiconductors and enabling spin-based devices.[1]

Recently, we described the new family of compounds $A_2Cd_3Q_4$ (A = K, Rb; Q = S, Se, Te)[9] that feature unique $[Cd_3S_4]^{2-}$ layers with cuboidal Cd_3S_4 cluster. The unique, low-dimensional structure and the possible superexchange paths in the $K_2Cd_3S_4$-type compounds have led us to a structural, optical, and magnetic study of $K_2Cd_{3(1-x)}Mn_{3x}S_4$ solid solutions, with $0 < x < 1$. Theoretically, Mn atoms would replace Cd atoms in the $(M_3S_4)_n^{2n-}$ layers. Each truncated cuboidal fragment in this layered structure contains three metal atoms connected together with S^{2-} ions. In each truncated cube the metals form an almost equilateral triangle with M−M distances of ∼3.2 Å. From a magnetic point of view the triangular geometry presents a degenerate ground state which could give rise to unusual magnetic phenomena.[10] Thus, increasing amounts of manganese could result in the phenomenon of "frustrated spins," leading to spin-glass-like behavior.[11] Other possible long-range ordering could include ferromagnetism, antiferromagnetism, or ferrimagnetism, as is observed in $Cd_{2-x}Mn_xP_2S_6$. In contrast to the behavior found in the systems described here, a similar study of solid solutions in the system $Cs_2Zn_{3(1-x)}Mn_{3x}S_4$, which does not possess truncated cuboidal clusters, indicated only antiferromagnetic ordering.[12] Here, we report in detail the synthesis of $K_2Cd_{3(1-x)}Mn_{3x}S_4$ solid solutions and describe the evolution of the structural, optical, photoluminescent, and magnetic properties of these compounds as a function of Mn. Interestingly, structural transitions are observed as a function of *x*. The compounds display both strong red emission, even at room temperature, and interesting magnetic behavior. We also describe the structure of $K_2Mn_3S_4$, which defines the end member of the series (i.e., $x = 1$) and has a surprising structure.

Experimental Section

$K_2Cd_{3(1-x)}Mn_{3x}S_4$ Solid Solutions. All the $K_2Cd_{3(1-x)}Mn_{3x}S_4$ solid solutions were produced by reacting stoichiometric amounts of Cd and Mn metals in excess K_2S_3. The details of the synthesis of each material are summarized in Table 1. A charge of 0.331 g (3.0 mmol) of K_2S, appropriate amounts of Cd metal and Mn metal, and 0.192 g (6.0 mmol) of elemental S was loaded into an alumina thimble. The thimble was then sealed inside a 13-mm-o.d. × 11-mm-i.d. carbon-coated silica tube. The tube was placed into a computer-controlled furnace, heated at 800 °C for 2 days, and then cooled at 2 °C/h to 700 °C and at 25 °C/h to 50 °C. The excess of K_2S_3 promoted crystal growth, prevented the formation of $Cd_{1-x}Mn_xS$, and was washed away with methanol. The $K_2Cd_{3(1-x)}Mn_{3x}S_4$ solid solutions were isolated with methanol under a nitrogen atmosphere. A 75% yield, based on Cd and Mn, is typical. The compounds are insoluble in H_2O and common organic solvents, but are sensitive to long exposure (several days) to air. The elemental compositions of all materials were verified by semiquantitative microprobe analysis on several crystals from each batch; see Table 1.

Table 1. Conditions for the Preparation of $K_2Cd_{3(1-x)}Mn_{3x}S_4$ Solid Solutions

x (nominal)	K_2S/S (mmol)	Cd (mmol)	Mn (mmol)	obsd composition by EDS analysis
0.0	3/6	6 g	0	$K_2Cd_3S_4$
0.05	3/6	5.7	0.3	$K_2Cd_{2.76}Mn_{0.19}S_4$
0.1	3/6	5.4	0.6	$K_2Cd_{3.3}Mn_{0.4}S_4$
0.2	3/6	4.8	1.2	$K_2Cd_{2.5}Mn_{0.6}S_4$
0.4	3/6	3.6	2.4	$K_2Cd_{1.8}Mn_{1.2}S_4$
0.6	3/6	2.4	3.6	$K_2Cd_{1.6}Mn_{1.4}S_4$
0.87	3/6	0.6	5.4	$K_2Cd_{0.2}Mn_{3.0}S_4$
1.0	3/6	0	6	$K_2Mn_3S_4$

Table 2. Lattice Parameters and Space Groups of the $K_2Cd_{3(1-x)}Mn_{3x}S_4$ Solid Solutions

x	*a* (Å)	*b* (Å)	*c* (Å)	volume (Å^3)	space group
0.0	13.880(4)	10.247(3)	6.608(1)	939.8(7)	*Pnma*
0.2	13.884(6)	10.224(4)	6.542(3)	928.6(7)	*Pnma*
0.4	13.863(4)	10.184(1)	6.480(1)	914.8(3)	*Pnma*
0.6	13.851(4)	10.139(2)	6.428(2)	902.7(4)	*Pnma*
0.87	5.9217(8)	13.531(1)	11.070(1)	887.0(1)	*Ccca*
0.88	5.890(1)	13.489(1)	11.066(1)	879.4(2)	*Ccca*
1.0	11.0637(7)	26.830(2)	5.818(1)	1727(1)	*Ccca*

$K_2Mn_3S_4$. A charge of 0.331 g (3.0 mmol) of K_2S, 0.330 g (6.0 mmol) of Mn metal, and 0.192 g (6.0 mmol) of elemental S was loaded into an alumina thimble, which was sealed inside a carbon-coated silica tube. The tube was heated at 800 °C for 2 days and then cooled at 2 °C/h to 700 °C and at 25 °C/h to 50 °C. The product was isolated as above. The compound is insoluble in H_2O and common organic solvents, but is sensitive to air exposure for several days. A yield of 60%, based on Mn, is typical.

Crystallographic Studies

Single-Crystal X-ray Diffraction. *$K_2Cd_{3(1-x)}Mn_{3x}S_4$ ($x \leq 0.6$).* Because for $x \leq 0.6$ the compounds have the structure of $K_2Cd_3S_4$ ($x = 0$), only the unit cells were determined at 23 °C; see Table 2. For the sample with $x = 0.6$ data collection and crystallographic refinement were performed to verify the structure; however, these details are not reported here.

$K_2Cd_{3(1-x)}Mn_{3x}S_4$ ($x = 0.87$, 0.88). Single-crystal X-ray diffraction data for $K_2Cd_{0.39}Mn_{2.61}S_4$ ($x = 0.87$) were collected on a Rigaku AFC6S four-circle diffractometer (Mo Kα radiation, graphite monochromated) at 23 °C. Cell parameters were $a = 5.922(1)$ Å, $b = 13.531(1)$ Å, $c = 11.070(1)$ Å, *Ccca*, and final $R/R_w = 0.046/0.089$. The crystal was stable, as judged by three check reflections measured every 150 reflections throughout the data set. The structure was solved by the direct methods routine of SHELXS-86[13] and refined by the full-matrix least-

(9) Axtell, E. A.; Liao, J.-H.; Kanatzidis, M. G. *Chem. Eur. J.* **1996**, *2*, 656−666.
(10) Suzuki, I. S.; Suzuki, M. *J. Phys.: Condens. Matter* **1999**, *11*, 521−541. (b) Cava, R. J.; Ramirez, A. P.; Huang, Q.; Krajewski, J. J. *J. Solid State Chem.* **1998**, *140*, 337−344. (c) Schiffer, P.; Daruka, I. *Phys. Rev. B* **1997**, *56*, 13712−13715. (d) Mentre, O.; Dhaussy, A. C.; Abraham, F.; Steinfink, H. *J. Solid State Chem.* **1997**, *130*, 223−233. (e) Zhang, W. M.; Saslow, W. M.; Gabay, M.; Benakli, M. *Phys. Rev. B* **1993**, *48*, 10204−10216. (f) Reimers, J. N.; Dahn, J. R.; Greedan, J. E.; Stager, C. V.; Liu, G.; Davidson, I., Vonsacken, U. *J. Solid State Chem.* **1993**, *102*, 542−552. (g) Reimers, J. N.; Greedan, J. E.; Bjorgvinsson, M. *Phys. Rev. B* **1992**, *45*, 7295−7306.
(11) Binder, K.; Young, A. P. *Rev. Mod. Phys.* **1986**, *58*, 801−976.
(12) Heming, M.; Lehmann, G. *Z. Naturforsch A* **1983**, *38*, 149−153. (b) Bronger, W.; Balkhardtdegen, H.; Muller, P. *Z. Kristallogr.* **1988**, *182*, 47−49.
(13) Sheldrick, G. M. In *Crystallographic Computing 3*; Sheldrick, G. M., Kruger, C., Doddard, R., Eds.; Oxford University Press: Oxford, England, 1985; pp 175−189.

Table 3. Summary of Crystallographic Data for $K_2Cd_{3(1-x)}Mn_{3x}S_4$

formula	$K_2Cd_{0.35}Mn_{2.65}S_4$	$K_2Mn_3S_4$
FW (g/mol)	391.51	371.26
color/habit	red/irreg	red/irregular plate
dimensions (mm)	0.30 × 0.22 × 0.12	0.46 × 0.26 × 0.08
a (Å)	5.890(1)	11.0637(7)
b (Å)	13.489(1)	26.830(2)
c (Å)	10.066(1)	5.8180(4)
V (Å^3)	879.4(2)	1727.0(2)
space group, Z	*Ccca*, 4	*Ccca*, 8
d_{calc} (g/cm^3)	2.957	2.856
μ(Mo Kα) (cm^{-1})	63.9	61.55
radiation	Mo Kα (λ = 0.71069 Å)	Mo Kα (λ = 0.71069) Å
temperature (°C)	−100	−100
scan type	$2\theta/\omega$	$2\theta/\omega$
$2\theta_{max}$ (deg)	55	55
min./max. absorption coeff. for ψ-scan correction	0.6/1.1	0.28/0.76
reflections measured	2532	3612
no. of reflections with $I > 3\sigma(I)$	547	787
no. variables	23	47
R/R_w[a]	0.046/0.14	0.081/0.20

[a] $R = \Sigma(|F_o| - |F_c|)/\Sigma|F_o| R_w = \{\Sigma w(|F_o^2| - |F_c^2|)^2/\Sigma w|F_o^2|^2\}^{1/2} w = 1/\sigma^2(F)$.

Table 4. Fractional Atomic Coordinates (×10^4), U_{eq}[a] Values and Site Occupancies for $K_2Cd_{0.35}Mn_{2.65}S_4$ with Estimated Standard Deviations in Parentheses

	x	y	z	U_{eq}[a]	occupancy
Cd1	0	2500	5398(7)	31(3)	0.18
Mn1	0	2500	5209(3)	9(1)	0.82
Mn2	0	2500	2500	5(1)	1.0
K	−7500	0	1289(1)	19(1)	1.0
S1	2211(2)	1430(1)	3835(1)	12(1)	1.0

[a] U_{eq} is defined as one-third of the trace of the orthogonalized $\mathbf{U}_{ij}$ tensor.

squares techniques of the TEXSAN package of crystallographic programs.[14] An empirical absorption correction based on ψ-scans was applied to the data set, followed by a DIFABS correction to the isotropically refined structure as recommended.[15] The structure was modeled satisfactorily with 13% Cd and 87% Mn on the two metal sites. All atoms were eventually refined anisotropically. To check for reproducibility, another sample (from a different synthesis batch) was also refined and gave $x = 0.88$. The data were collected with a SMART Platform CCD diffractometer as described below. The structural model was identical to that of the $x = 0.87$ sample. Because of the substantially identical results obtained, the complete parameters and details of the structure solution and refinement are given only for $K_2Cd_{0.35}Mn_{2.65}S_4$; see Table 3. The coordinates of all atoms, isotropic equivalent temperature factors, and their standard deviations are given in Table 4.

$K_2Mn_3S_4$. The structure of this compound was recently described by Bronger et al. albeit we believe in an incorrect unit cell and space group.[16] $K_2Mn_3S_4$ was reported to crystallize in the monoclinic space group $P2/c$, with $a = 7.244(2)$ Å, $b = 5.822(1)$ Å, $c = 11.018(5)$ Å, $\beta = 112.33(3)°$, and $Z = 2$. The $[Mn_3S_4]$ layers were described to be of the [PbO] type with disordered vacancies in the Mn sites. Our results differ from their conclusions in that we have observed a superstructure over that described by the monoclinic structure.

The crystals of $K_2Mn_3S_4$ did not diffract well and at first we were not able to collect good diffraction data for this material using conventional serial four-circle diffractometers. Only the cell parameters of $K_2Mn_3S_4$ could be determined which were the same as those reported by Bronger. Though data were collected with a four-circle diffractometer, the structure could not be solved in a satisfactory manner, partly because of the broad and weak nature of the diffraction peaks and partly because of the Mn atom disorder. During the course of this work the Department of Chemistry was equipped with a Siemens SMART Platform CCD diffractometer which proved to be crucial in eventually determining the structure of $K_2Mn_3S_4$. This is because weak reflections could be better measured and we were able to observe a considerably larger orthorhombic cell (4× larger than the monoclinic one); see Table 3. A full reciprocal lattice sphere of data was recorded to a resolution of 0.75 Å. Three major swaths of frames were collected with 0.30° steps in ω and an exposure time of 20 s/frame, giving a total measurement time of <10 h. An initial cell was obtained using the SMART program.[17] The SMART program was used to extract reflections from 300 frames of the actual data collection. From the reflections extracted the strongest 80 were used to find an initial cell. This cell was used to integrate the data using the SAINT program.[17] The final cell constants were determined from a set of 746 strong reflections obtained from data collection. The absorption correction was done using SADABS[18] and all refinements were done using the SHELXTL[18] package of crystallographic programs. Systematic absence conditions of the data set gave space group, *Ccca*. The structure was solved with direct methods using SHELXTL. The calculations were performed on a Silicon Graphics Iris Indigo workstation. Refer to Table 3 for a summary of crystallographic data. See Table 5 for positional parameters, isotropic temperature factors, and site occupancies for $K_2Mn_3S_4$.

Table 5. Fractional Atomic Coordinates (×10^4), U_{eq}[a] Values and Site Occupancies for $K_2Mn_3S_4$

	x	y	z	U_{eq}[a]	occupancy
Mn1	5000	2500	2500	7(1)	1.0
Mn2	2280(1)	2500	2500	9(1)	1.0
Mn3	0	3(1)	7500	36(1)	1.0
Mn4	2500	0	−2506(4)	17(1)	0.50
K	1235(2)	1252(1)	75(2)	22(1)	1.0
S1	1327(1)	1969(1)	5314(3)	11(1)	1.0
S2	1173(2)	533(1)	4988(3)	24(1)	1.0

[a] U_{eq} is defined as one-third of the trace of the orthogonalized $\mathbf{U}_{ij}$ tensor.

Physical Measurements

Semiquantitative Microprobe Analysis. Semiquantitative microprobe analysis was performed on a JEOL JSM-6400 SEM equipped with a Noran energy dispersive spectroscopy (EDS) system. Data acquisition was performed with an accelerating voltage of 20 kV. Compositions given in Table 1 are the average of values obtained from several crystals.

Powder X-ray Diffraction. The compounds were examined by X-ray powder diffraction to check phase purity. Powder patterns obtained with Cu Kα radiation on a Philips XRG-3000 powder diffractometer and a rotating anode X-ray powder diffractometer, Rigaku-Denki/Rw400F2 (RotaFlex), provided accurate d_{hkl} spacings and showed that materials with $x \leq 0.6$ are X-ray isomorphous to the end member, $K_2Cd_3S_4$.

Absorption Spectroscopy. A Shimadzu UV-3101PC double-beam, double-monochromator spectrophotometer was used to measure the room temperature, optical diffuse reflectance spectra of the compounds. The methods used to collect the reflectance data and convert it to absorbance values have

(14) TEXSAN: Single-Crystal Structure Analysis Software, Version 5.0; Molecular Structure Corp.: The Woodlands, TX, 1981.
(15) Walker, N.; Stuart, D. *Acta Crystallogr.* **1983**, *39A*, 158.
(16) Bronger, W.; Bohmer, M.; Schmitz, D. *Z Anorg. Allg. Chem.* **2000**, *626*, 6−8.
(17) SMART and SAINT. Data Collection and Processing Software for the SMART System; Siemens Analytical X-ray Instruments Inc.: Madison, WI, 1995.
(18) SHELXTL V-5; Siemens Analytical X-ray Systems Inc.: Madison, WI.

been described elsewhere.[19] We have obtained the band gap values by extrapolating the linear regions of each $(\alpha/S)^2$ versus energy plot to $(\alpha/S)^2 = 0$.[20]

Photoluminescence Spectroscopy. Photoluminescence spectra for the compounds were obtained on a Spex Fluorolog-2, Model F111A1 spectrofluorometer. Excitation wavelengths were chosen from a 150-W xenon arc lamp by means of a single grating spectrometer. This spectrometer was equipped with a 1200 groove/mm diffraction grating and 5-nm band-pass slits. The sample compartment was equipped with a vertically mounted liquid nitrogen Dewar. Emitted light was collected in the "front face" mode, 22.5° away from the incident beam. Emission wavelengths were selected with a single grating spectrometer, equipped with a 1200 groove/mm diffraction grating and 1.0-nm band-pass slits. The signal was detected with a Hamamatsu R928 photomultiplier. Excitation spectra were corrected for lamp intensity by comparison with a quantum counter reference detector loaded with Rhodamine B. Powdered samples were loaded in 3-mm silica tubing and sealed under vacuum (approximately 1.0×10^{-4} mbar).

Differential Thermal Analysis (DTA). Thermal analysis was performed on a Shimadzu DTA-50 differential thermal analyzer. High-quality crystals were selected from the reaction product and ground. Approximately 15−20 mg of each material was loaded into a 2.0-mm-i.d. × 3.0-mm-o.d., carbon-coated silica tube with a flattened bottom and sealed under a vacuum of less than 1×10^{-4} mbar. A carbon-coated tube filled with 20 mg of Al_2O_3 powder was used as the reference. Heating and cooling rates of 10 °C/min were used. Typically, the samples showed an endothermic peak upon heating and an exothermic peak upon cooling. The temperature associated with each thermal event was assigned to the melting and recrystallization, respectively. Comparisons between x-ray powder patterns taken before and after heating were made to establish congruent melting.

Magnetic Susceptibility Measurements. Several independent magnetic measurements have been made on the $K_2Cd_{3(1-x)}Mn_{3x}S_4$ solid solutions. These include the following: the temperature dependence of the dc magnetization, the temperature dependence of the ac magnetization, and the magnetic field dependence of the magnetization at a fixed temperature. Each of these measurements gives different, but complementary, information about how the magnetic properties change with increasing Mn concentration. The measurements were done on a MPMS Quantum Design superconducting quantum interference device (SQUID). For each sample, 20−80 mg of the compound was ground, loaded into a plastic bag (<8 cm^2), and sealed on a Seal-a-Meal bag sealer.

The temperature dependence of the dc magnetization was obtained in the following manner. One data set was obtained by first cooling the sample in a 0-G applied field and then applying a measuring field of 100−1000 G. The data were collected with increasing temperature from 5 to 300 K, with 2−5 K intervals between 5 and 100 K and 20 K intervals between 100 and 300 K. These are the zero-field-cooled (ZFC) data and are followed by another data set obtained by first cooling the sample in the measuring field and then collecting data with increasing temperature, as above. This provided the field-cooled (FC) data.

ac susceptibility data were obtained at intervals of 2 K, from 5 to 50 K. At each temperature, an oscillating field with an amplitude of 1 G was applied. The oscillating field was driven at frequencies of 1000, 100, 10, and 1 Hz. Both the in-phase magnetization and the out-of-phase magnetization were determined at each temperature and frequency.

Hysteresis curves of magnetization versus field were determined by cycling the field from 0 to 10 000 G (1 T) to −10 000 G and back to 10 000 G. The measurements were normally made with intervals of 100 G from 0 to 10 000 and intervals of 1000 G at higher fields. All data reported were taken at 5 K.

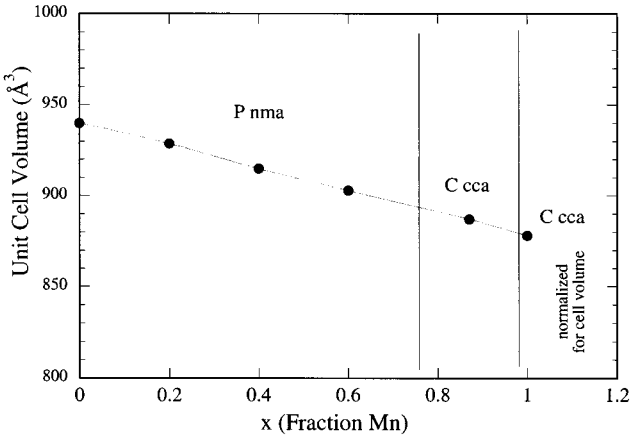

Figure 1. Unit cell volumes as a function of x for the $K_2Cd_{3(1-x)}Mn_{3x}S_4$ solid solutions.

Results and Discussion

Structure Description. The unit cell volumes of the $K_2Cd_{3(1-x)}Mn_{3x}S_4$ solid solutions obey Vegard's Law; see Figure 1. Therefore, to a first approximation the smaller manganese atoms are inserting into the parent $K_2Cd_3S_4$ structure[9] in a random manner. This random substitution occurs up to a value of $x = 0.6$, at which point a structural change occurs. For the $x \leq 0.6$ samples, the cell parameters decrease in length with increasing Mn content; see Table 2. The crystallographic *a*-axis of the $x = 0.6$ compound is 0.21% shorter than the $x = 0.0$ compound. The crystallographic *b*-axis is shortened by 1.05% over the same range and the crystallographic *c*-axis decreases by 2.72%. The crystallographic *b*- and *c*-axes are the dimensions of the infinite layer and vary more substantially with increasing Mn content. In contrast, the *a*-axis is perpendicular to the layers and is relatively insensitive.

Materials with $x \leq 0.6$. The compounds with $x \leq 0.6$ are composed of $(M_3S_4)_n^{2n-}$ layers which were described in detail earlier;[9] see Figure 2. They are composed of cuboidal cup-shaped $[M_3S_4]^{2-}$ clusters with a μ_3-S atom (S2) at the apex of the cube. The remaining three S atoms (S1 and S3) are also μ_3-type but they bond to two metal atoms of the same cluster and one metal atom in an adjacent cluster. The clusters are arranged in rows along the *c*-axis. Within each row, the clusters point in the same direction. Rows of clusters are arranged side by side, pointing in opposite directions as the *b*-axis is traversed. Each cluster has six neighboring clusters, two of which point in the same direction and four which point in the opposite direction (Figure 2A). The Cd and Mn atoms are in distorted tetrahedral coordination (due to the presence of the three four-membered rings within the defect cube).

For later discussions of super-exchange, it is important to consider here how each metal atom is situated with respect to its six, in-plane nearest neighbors. Neighboring metal atoms within the same cluster are at ~3.24 and ~3.39 Å apart. The nearest M neighbors in adjacent clusters are ~3.8 Å away; see Figure 2B. The distance between $[M_3S_4]^{2-}$ layers is ~6.9 Å; there-

(19) McCarthy, T. J.; Ngeyi, S.-P.; Liao, J.-H.; DeGroot, D. C.; Schindler, J.; Kannewurf, C. R.; Kanatzidis, M. G. *Chem. Mater.* **1993**, *5*, 331−340.

(20) Pankove, J. I. In *Optical Processes in Semiconductors*; Dover Publications: New York, 1975.

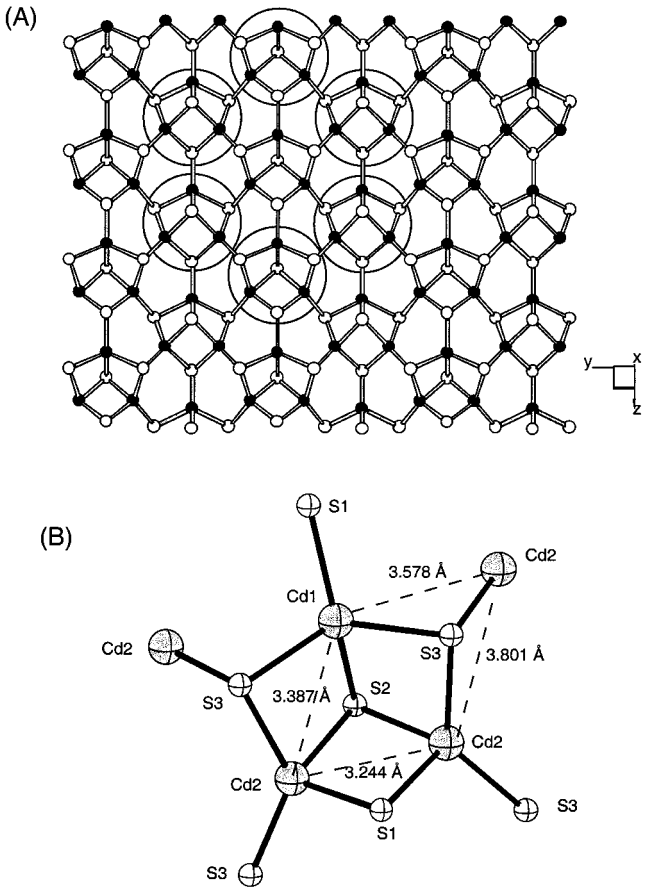

Figure 2. (A) A view perpendicular to one $[Cd_{3(1-x)}Mn_{3x}S_4]_n^{2n-}$ layer in the $K_2Cd_{3(1-x)}Mn_{3x}S_4$ solid solutions with $x \leq 0.6$ (M, filled circles; S, open circles). The shaded circles placed over the M_3S_4 clusters are meant to highlight the pseudohexagonal arrangement of these clusters within a slab. (B) A single cuboidal cluster with some of the magnetically relevant M−M distances shown. This cluster is cup-shaped with S2 atom at the bottom.

fore, M−M distances are too long for significant magnetic interactions.

The $x \sim 0.88$ Material. Two slightly different compositions (obtained from two different batches) were refined to $K_2Cd_{0.39}Mn_{2.61}S_4$ ($x = 0.87$) and $K_2Cd_{0.35}Mn_{2.65}S_4$ ($x = 0.88$); see Table 3. Both gave very similar behavior. These compositions adopt the $Cs_2Zn_3S_4$ structure,[21] which is one of the five layered structure types with the $A_2M_3Q_4$ formula. Four of these, except the $K_2Cd_3S_4$-type, are related to the $ThCr_2Si_2$[22] structure type. The $(M_3Q_4)_n^{2n-}$ layers feature a defect anti-PbO structure, where one-quarter of the metal atoms has been removed. In the $Cs_2Zn_3S_4$ structure, the defects are arranged in an ordered manner, in staggered rows. In $Cs_2Ag_2ZrTe_4$,[23] the vacancies rearrange into a nearly square lattice which is $2a \times 2a$ larger than the original $ThCr_2Si_2$ structure. A third structure with the $A_2M_3Q_4$ stoichiometry is $A_2Cd_3Te_4$,[24] (A = K, Rb, Cs) which

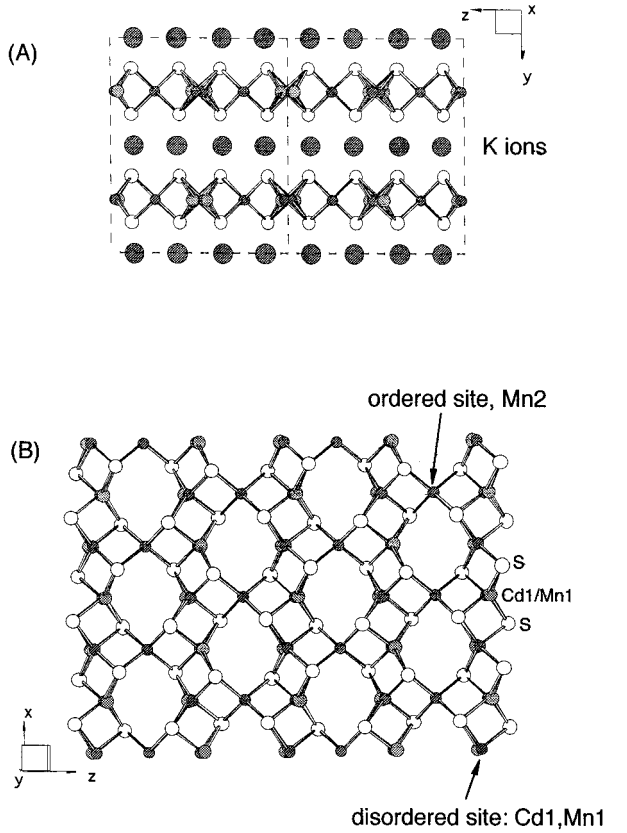

Figure 3. View (A) parallel and (B) perpendicular to one $[Cd_{3(1-x)}Mn_{3x}S_4]_n^{2n-}$ layer in the $K_2Cd_{0.35}Mn_{2.65}S_4$ ($x = 0.88$) solid solution (M, filled circles; S, open circles).

adopts a unit cell similar to that of $ThCr_2Si_2$ but charge balance requires that one-fourth of the metal atoms be removed. All $A_2M_3Q_4$ compounds are layered with distorted tetrahedral coordination about the metal.

The structure of $K_2Cd_{0.35}Mn_{2.65}S_4$ is shown in Figure 3. The layers are arranged perpendicular to the crystallographic *b*-axis. Within each layer vacancies are ordered arranged in rows along the crystallographic *a*-axis, resulting in eight-membered, M_4S_4 holes. The rows of holes are staggered in the crystallographic *c*-direction. Whereas in $Cs_2Zn_3S_4$ the layers are stacked such that the holes are aligned in the perpendicular direction, in $K_2Cd_{0.35}Mn_{2.65}S_4$ the layers shift by half the crystallographic *a*-constant so they are no longer aligned. The Cd atoms remain in (0, $^1/_2$, *z*) sites and are disordered with Mn1 atoms lying in parallel rows along the *a*-axis; see Figure 3. These are distorted tetrahedral sites but are less distorted than those of the $K_2Cd_3S_4$-type compounds; see Table 6. Interestingly, the Cd/Mn distribution in the structure does not seem to be totally random as there is one pure Mn site and one mixed Mn/Cd site in the crystal. We note that we cannot rule out the fact that the apparent Cd/Mn disorder in this structure is not an artifact arising from the presence of some superstructure.

The Structure of $K_2Mn_3S_4$ ($x = 1$). The structure of this compound is different from that of $Cs_2Mn_3S_4$ and also from that of $K_2Cd_3S_4$ as it does not contain $(M_3S_4)^{2-}$ clusters. The structure is also unusual in that it contains two different types of alternating Mn_3S_4 layers, shown in Figure 4. Both are derivatives of the anti-PbO structure type, one of which contains *ordered* vacancies

(21) Bronger, W.; Hendriks, U. *Rev. Chim. Miner.* **1980**, *17*, 555−560.
(22) Leciejewicz, J.; Siek, S.; Szytula, A. *J. Less Common Met.* **1988**, *144*, L9−L13.
(23) Pell, M. A.; Ibers, J. A. *J. Am. Chem. Soc.* **1995**, *117*, 6284−6286.
(24) Axtell, E. A. Ph.D. Dissertation, 1995, Michigan State University, East Lansing, MI. (b) Narducci, A. A.; Ibers, J. A. *J. Alloy Compd.* **2000**, *306*, 170−174.

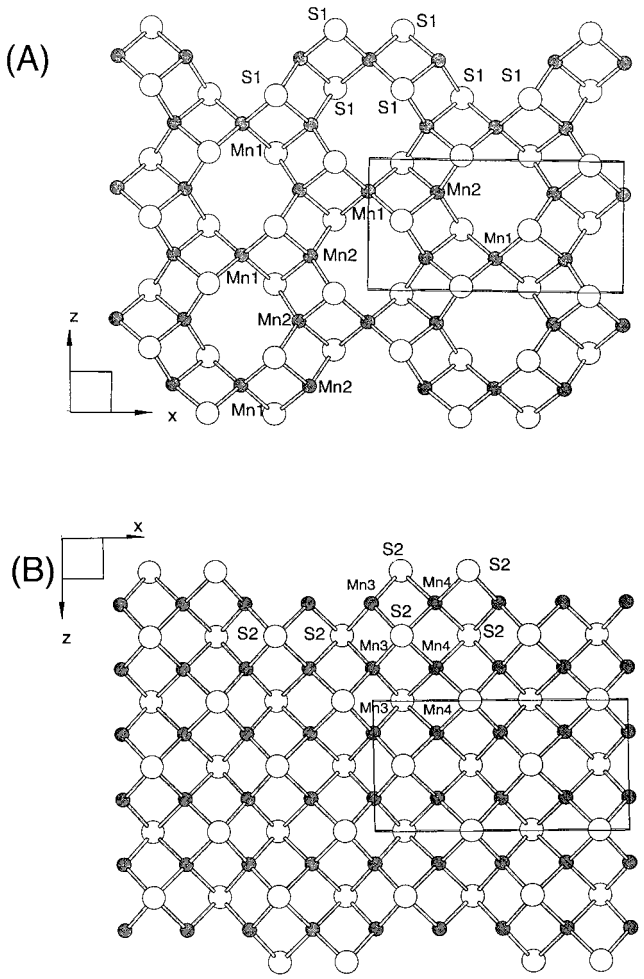

Figure 4. Two individual layers in $K_2Mn_3S_4$. The layers derive from the anti-PbO [MnS] layer by removing one-fourth of the Mn atoms. (A) Layer in which the Mn vacancies are ordered. (B) Layer in which the Mn vacancies are random.

Table 6. Selected Bond Distances and Bond Angles for $K_2Cd_{0.35}Mn_{2.65}S_4$ ($x = 0.88$) with Standard Deviations in Parentheses

bond	distance	angle	value
M1−Mn2	3.853(2) Å	S1−M1−S1	105.4(1)°
M1−Mn2	3.070(2) Å	S1−M1−S1	115.3(1)°
M2−Mn2	3.022(1) Å	S1−M1−S1	107.9(1)°
M1−S1	2.444(3) Å	S1−M2−S1	131.6(2)°
Mn2−S1	2.402(3) Å	S1−M2−S1	105.9(1)°
Mn2−S1	2.511(3) Å	S1−M2−S1	104.12(9)°
		S1−M2−S1	101.5(2)°
K1−S1	3.466(3) Å		
K1−S1	3.689(3) Å	M1−S1−M2	76.6(1)°
K1−S1	3.400(3) Å	M1−S1−M2	105.3(1)°
K1−S1	3.308(3) Å	M2−S1−M2	75.88(9)°

with one-fourth of the Mn atoms missing and one which contains *disordered* vacancies with one-fourth of the Mn atoms missing.[25] This is a rather surprising result because the structure of $K_2Cd_{0.35}Mn_{2.65}S_4$ adopts essentially a subcell of that of $K_2Mn_3S_4$ with half the volume, yet it presents ordered vacancies. Further, it is not obvious what are the stabilizing factors responsible for the presence of both types of Mn_3S_4 layers in the same lattice when one such layer in the $K_2Cd_{0.35}Mn_{2.65}S_4$ motif would suffice. Therefore, the possibility of a superstructure that will order the vacancies in $K_2Mn_3S_4$ cannot be excluded at this time.

(25) It is quite possible that these vacancies are actually ordered as well, but in different domains in the structure. This will result in a superstructure, which however we have not identified. The observation of any superstructure is complicated by the poor growth habit of the crystals. A clue as to this possibility is provided by the very large U11 anisotropic temperature factor of Mn(3).

Table 7. Selected Bond Distances and Bond Angles for $K_2Mn_3S_4$ with Estimated Standard Deviations in Parentheses

bond	distance (Å)	bond	distance (Å)
Mn1−Mn2	3.8501(14)	M3−M4	2.7659(2)
Mn1−Mn2	3.0098(14)	M3−M3	2.9091(2)
Mn2−Mn2	2.9496(5)		
Mn1−S1	2.408(2)	M3−S2	2.416(2)
Mn2−S1	2.413(2)	M3−S2	2.418(2)
Mn2−S1	2.454(2)	M4−S2	2.511(2)
		M4−S2	2.515(2)
K1−S1	3.434(3)	K1−S2	3.290(3)
K1−S1	3.606(2)	K1−S2	3.450(2)
K1−S1	3.374(2)	K1−S2	3.457(3)
K1−S1	3.316(2)	K1−S2	3.534(2)
angle	value (deg)	angle	value (deg)
S1−Mn1−S1	104.89(8)	S2−Mn3−S2	106.00(6)
S1−Mn1−S1	116.26(9)	S2−Mn3−S2	115.06(9)
S1−Mn1−S1	107.50(8)	S2−Mn3−S2	108.00(11)
S1−Mn2−S1	128.18(10)	S2−Mn4−S2	108.49(8)
S1−Mn2−S1	105.39(5)	S2−Mn4−S2	109.40(11)
S1−Mn2−S1	106.48(7)	S2−Mn4−S2	110.67(9)
S1−Mn2−S1	102.14(9)		
Mn1−S1−Mn2	76.48(6)	Mn3−S2−Mn4	68.21(5)
Mn1−S1−Mn2	106.00(7)	Mn3−S2−Mn4	68.25(5)
Mn2−S1−Mn2	74.61(5)	Mn3−S2−Mn4	108.80(9)
		Mn4−S2−Mn4	70.74(5)

The stacking sequence of the Mn_3S_4 layers is shown in Figure 5. In the course of attempting to elucidate the crystal structure of $K_2Mn_3S_4$, we encountered many problems. These include difficulty in identifying suitable single crystals, failure to initially determine the correct size of the unit cell (a monoclinic subcell was routinely seen), and inability to obtain an ordered structure despite a large number of independent data sets collected using a serial four-circle diffractometer. In retrospect, we attribute this to probable stacking faults and defects as well as microtwinning in which the two different types of Mn_3S_4 layers may occur randomly. Finally, the structure reported here was solved from data obtained using a CCD area detector. Selected bond distances and angles are given in Table 7.

Optical Absorption Spectroscopy

At low values of x, the $K_2Cd_{3(1-x)}Mn_{3x}S_4$ solid solutions are light yellow in color. The color grows darker, progressing through brown orange to red, with increasing manganese content. The band gap E_g of the end member $K_2Cd_3S_4$ is 2.75 eV. Up to $x = 0.2$ the band gap remains almost unchanged. The single-crystal absorption spectra of the $x \sim 0.05$ and 0.1 samples are shown in Figure 6A.

The absorption spectra of the $K_2Cd_{3(1-x)}Mn_{3x}S_4$ solid solutions with $x \sim 0.2$, 0.4, and 0.6 were obtained by powder diffuse reflectance spectroscopy; see Figure 6B. The spectra display steep absorption edges that are the result of charge-transfer excitations between an S

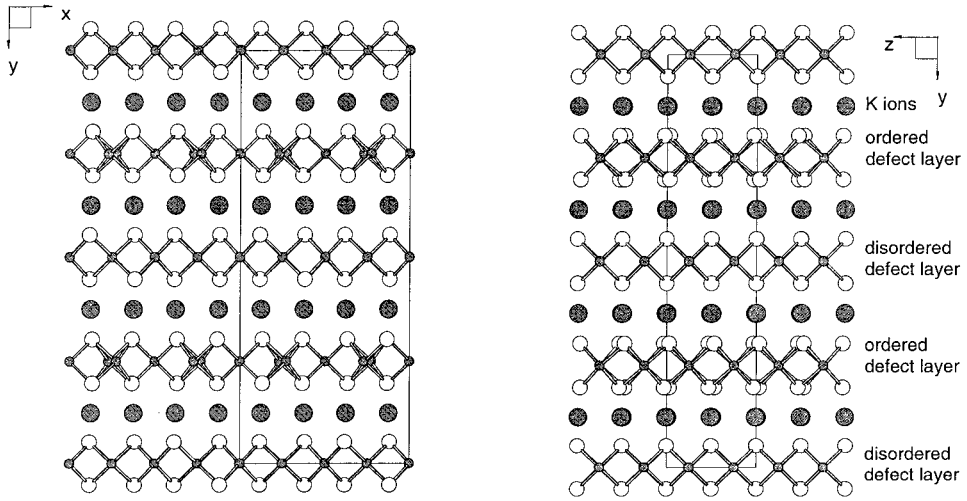

Figure 5. Two views of the layered structure of $K_2Mn_3S_4$.

p-based valence band and an Cd(Mn)-based conduction band. The band gaps increase slightly at $x = 0.4$ (~2.75 eV) and $x = 0.6$ (~2.80 eV). Along with the change in structure type at $x \sim 0.87$, a larger increase in the band gap is observed at ~3.0 eV; see Figure 6C. The sharp absorption edges of $K_2Cd_{3(1-x)}Mn_{3x}S_4$ and the observation of bright luminescence would suggest that the band gaps of these pseudo-ternaries are also most likely direct. Band structure calculations on $K_2Cd_3S_4$ at the extended Hückel level (tight binding approximation) indeed suggest the presence of a *direct* band gap at the Brillouin zone center.[26] The top of the valence band is made primarily of S p-type orbitals while the bottom of the conduction band is composed of predominantly s- and p-type Cd orbitals. Therefore, any optical transitions involve symmetry-allowed charge-transfer excitations from S to Cd.

As the Mn content increases in $K_2Cd_{3(1-x)}Mn_{3x}S_4$, weak absorption features are seen below the band-gap transitions. This we attribute to mid-gap states associated with Mn-based d−d transitions, which seem to play a significant role in the photoluminescence of these materials. In general, the band gaps of $K_2Cd_{3(1-x)}Mn_{3x}S_4$ solid solutions are larger than those of CdS. This is a result of the lower dimensional nature of the ternary compounds and has been discussed earlier.[9]

The end member $K_2Mn_3S_4$ showed an ill-defined band-gap transition. Its absorption spectrum is rather broad and an accurate E_g value was difficult to obtain. Its air sensitivity during the experiment further complicated an accurate determination of E_g.

Photoluminescence

The $K_2Cd_{3(1-x)}Mn_{3x}S_4$ solid solutions exhibit bright red photoluminescence at room temperature when excited with light above the band gap. Interestingly, at 77 K, the photoluminescence is markedly different for each of these solid solutions. The end member $K_2Mn_3S_4$ ($x = 1.0$) displayed no luminescence at room temperature or 77 K. For comparison purposes the luminescence behavior of the end member $K_2Cd_3S_4$ ($x = 0$) is described first.

(26) Sportouch, S.; Kanatzidis, M G., unpublished results.

$K_2Cd_3S_4$. With an exciting line of 3.12 eV (397 nm), this compound showed intense red emission at room temperature, with a maximum at 1.92 eV (646 nm); see Figure 7. In addition, a weak emission peak was observed at 2.41 eV (514 nm). Because the room-temperature band gap of $K_2Cd_3S_4$ is 2.75 eV (451 nm), light emission at 1.92 eV cannot be attributed to band-to-band luminescence and it probably arises from mid-gap defect states. This could be envisioned through electron excitation across the band gap followed by nonradiative relaxation to the mid-gap states and subsequent radiative relaxation to the ground state. Such emissive states could arise either from adventitious impurities or from structural defects (vacancies etc.) in the lattice. The room-temperature excitation spectrum of $K_2Cd_3S_4$, detected at 1.92 eV, displayed a maximum at 3.12 eV (397 nm) which fell rapidly to zero at approximately 2.95 eV (420 nm). This value is close to the energy band gap determined by optical absorption.

Upon cooling to 77 K, a fascinating result was observed. First, with an exciting line of 3.12 eV (397 nm), the same (but much sharper) red emission (1.92 eV, 646 nm) was obtained; see Figure 8A. Upon collection of an excitation profile with $E_{det} \sim 1.92$ eV ($\lambda_{det} =$ 646 nm), two intensity drops were observed, with edges at 3.31 eV (375 nm) and 3.12 eV (397 nm). When the exciting line was changed to 3.31 eV (375 nm), a change of only 0.19 eV (22 nm), a drastic color change in the emission from red to intense yellow was observed. The intensity of the 1.92 eV (646 nm) peak was dramatically reduced and the peak at 2.41 eV (514 nm) became very strong; see Figure 8B. An excitation profile recorded with $E_{det} \sim 2.41$ eV ($\lambda_{det} = 514$ nm) showed only the band with an edge at 3.31 eV (375 nm). Here, the emission fell to zero below 3.17 eV (391 nm). It would appear that there are two, rather than one, closely lying conduction bands (one at 3.12 and one at 3.31 eV) in which to excite electrons. At low temperatures, that is, 77 K, the higher energy band seems to participate more efficiently in the relaxation process, which involves a different emitting center at 2.41 eV. It would be interesting to further investigate the electronic structure of this compound.

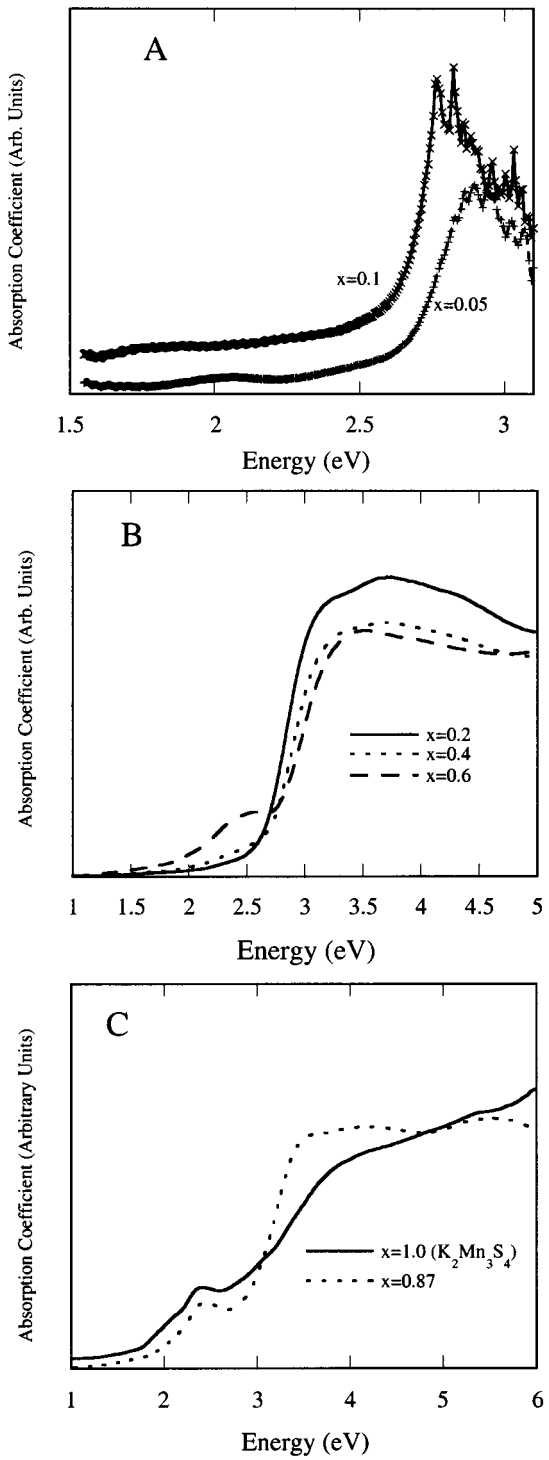

Figure 6. (A) Single-crystal absorption spectra for the $K_2Cd_{3(1-x)}Mn_{3x}S_4$ solid solutions with $x = 0.05$ and $x = 0.1$. (B) Absorption spectra for the $K_2Cd_{3(1-x)}Mn_{3x}S_4$ solid solutions with $x = 0.2$, 0.4, and 0.6 (powder samples). (C) Absorption spectra for the $K_2Cd_{3(1-x)}Mn_{3x}S_4$ solids solutions with $x = 0.87$ and 1.0 (powder samples).

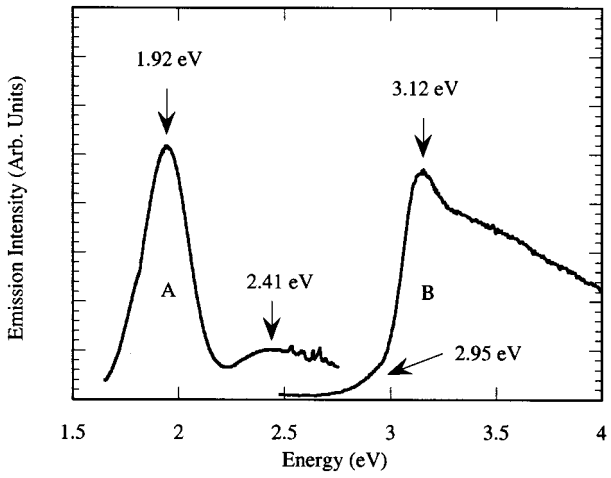

Figure 7. Room-temperature photoluminescence spectra of $K_2Cd_3S_4$: (A) Emission, $E_{exc} = 3.12$ eV. (B) Excitation, $E_{det} = 1.92$ eV.

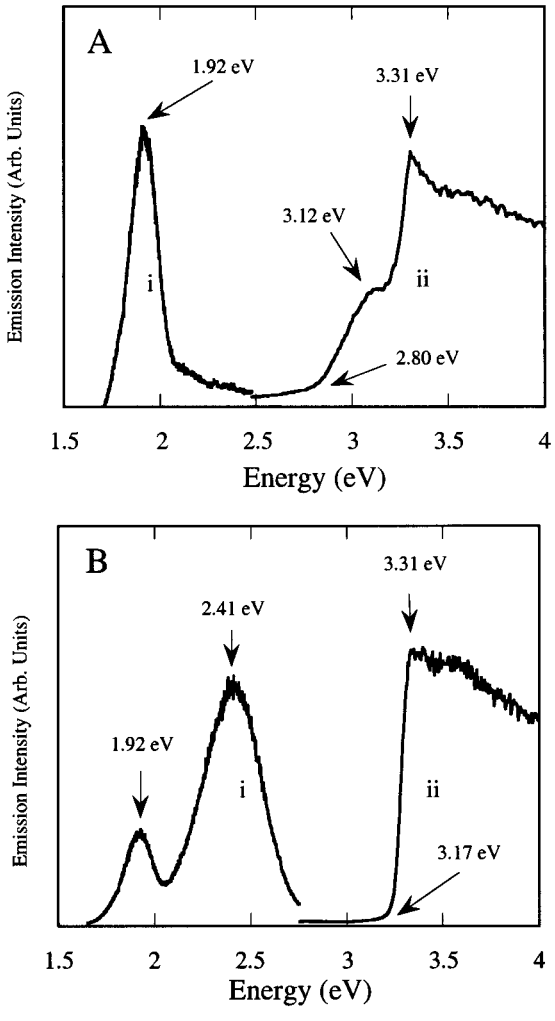

Figure 8. Photoluminescence spectra of $K_2Cd_3S_4$ at 77 K: (A) Emission (i), $E_{exc} = 3.12$ eV; excitation (ii), $E_{det} = 1.92$ eV. (B) Emission (i), $E_{exc} = 3.31$ eV.; excitation (ii), $E_{det} = 2.41$ eV.

$K_2Cd_{2.85}Mn_{0.15}S_4$ ($x = 0.05$). With an exciting line of 3.12 eV (375 nm), this compound showed intense red emission at room temperature, with two closely spaced maxima at 1.78 eV (697 nm) and 1.84 eV (675 nm); see Figure 9A. These two maxima occur at lower energy than the emission band of the parent compound. This peak shift may indicate the presence of a new mechanism for luminescence, introduced by the presence of the manganese atoms. The room-temperature excitation spectrum of $K_2Cd_{2.85}Mn_{0.15}S_4$ was detected at 1.84 eV (675 nm) and displayed a maximum at 3.12 eV (375 nm). This was followed by a shoulder at 2.92 eV (425 nm) and a rapid drop to approximately 2.69 eV (461 nm). Then, a second band at lower energy was observed with

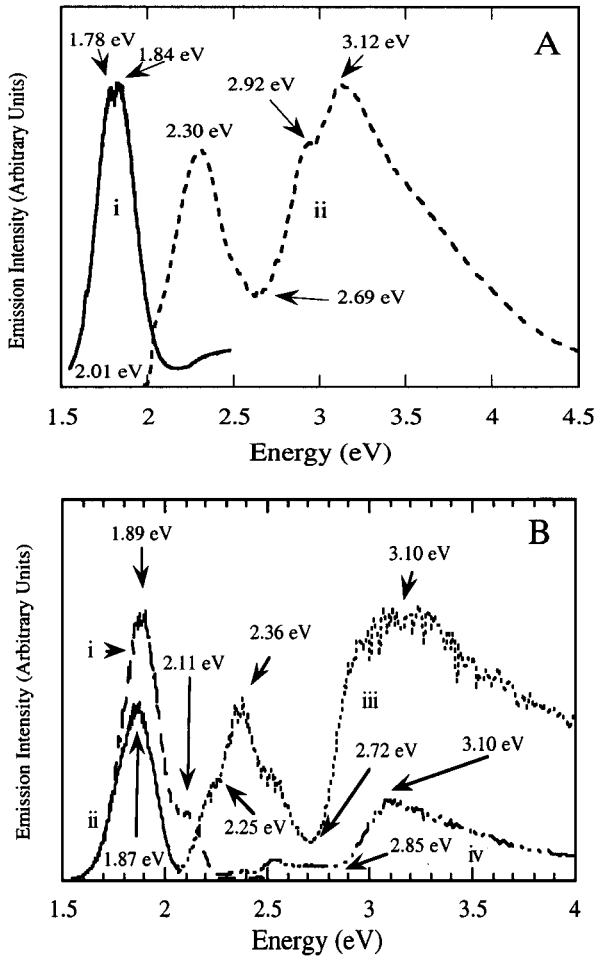

Figure 9. (A) Room-temperature photoluminescence spectra of $K_2Cd_{2.85}Mn_{0.15}S_4$ ((i) Emission, $E_{exc} = 3.12$ eV; (ii) excitation, $E_{det} = 1.84$ eV). (B) 77 K photoluminescence spectra of $K_2Cd_{2.85}Mn_{0.15}S_4$: ((i) Emission, $E_{exc} = 3.10$ eV; (ii) emission, $E_{exc} = 2.36$ eV; (iii) excitation, $E_{det} = 1.88$ eV; (iv) excitation, $E_{det} = 2.11$ eV).

a maximum at 2.30 eV (539 nm). This band falls to zero at 2.01 eV (617 nm), well below the band gap determined by optical absorption.

When excited with 3.10 eV (404 nm) light at 77 K, $K_2Cd_{2.85}Mn_{0.15}S_4$ showed intense red luminescence with a shoulder at 2.11 eV (590 nm) and a single maximum at 1.89 eV (658 nm); see Figure 9B. Both the shoulder and the peak itself occur at different energies than those observed for $K_2Cd_3S_4$. The 77 K excitation spectrum of $K_2Cd_{2.85}Mn_{0.15}S_4$ was detected at 1.88 eV (658 nm) and revealed a maximum at 3.10 eV (404 nm), followed by a drop in intensity to 2.72 eV (456 nm). With continued scanning to lower energies, a second band is observed at 2.36 eV (525 nm) with shoulders on both sides, at 2.50 eV (496 nm) and 2.25 eV (551 nm). This second band drops to zero by 2.11 eV (590 nm). The higher energy band at 3.12 eV is similar to that of the parent compound and it is tentatively assigned to a S to Cd charge transfer. The lower energy band is new and could result from transitions involving the Mn d-orbitals. An emission spectrum obtained with an exciting line of 2.36 eV (525 nm) only displays the red luminescence, with a maximum at 1.87 eV (663 nm). An excitation spectrum detected at 2.11 eV (588 nm) was generally weaker, with the lower energy band at 2.36 eV diminished in relative intensity.

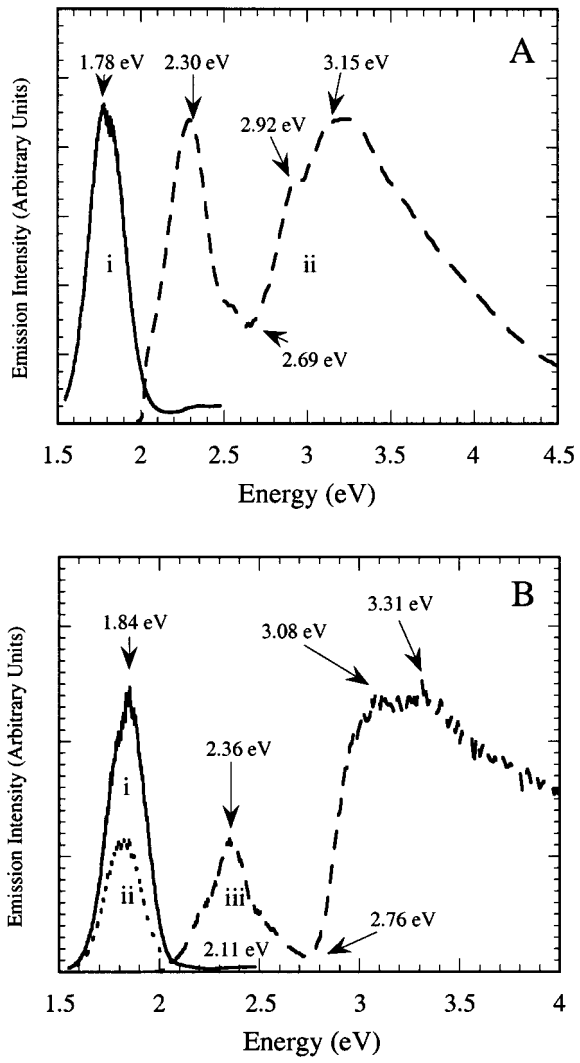

Figure 10. (A) Room-temperature photoluminescence spectra of $K_2Cd_{2.7}Mn_{0.3}S_4$: ((i) Emission, $E_{exc} = 3.15$ eV; (ii) excitation, $E_{det} = 1.78$ eV). (B) 77 K photoluminescence spectra of $K_2Cd_{2.7}Mn_{0.3}S_4$ ((i) Emission, $E_{exc} = 3.31$ eV; (ii) emission, $E_{exc} = 2.36$ eV; (iii) excitation, $E_{det} = 1.84$ eV).

$K_2Cd_{2.7}Mn_{0.3}S_4$ ($x = 0.1$). The room-temperature photoluminescence spectra of $K_2Cd_{2.7}Mn_{0.3}S_4$ ($x = 0.1$) are very similar to those of the $x = 0.05$ compound. With an exciting line of 3.15 eV (394 nm), $K_2Cd_{2.7}Mn_{0.3}S_4$ showed the same red emission, with maxima at 1.78 eV (697 nm) and 1.84 eV (675 nm); see Figure 10A. In this case, the emission peak changes a bit in shape, with the 1.78-eV peak slightly more intense than the 1.84-eV peak. The room-temperature excitation spectrum of $K_2Cd_{2.7}Mn_{0.3}S_4$ was detected at 1.78 eV (697 nm) and displayed a maximum at 3.15 eV (394 nm) which fell rapidly to a local minimum at approximately 2.69 eV (461 nm). In a manner similar to the $x = 0.05$ sample, a second peak was also observed with a maximum at 2.30 eV (539 nm). This band rapidly falls to zero by 2.00 eV (620 nm).

When excited with 3.31 eV (370 nm) light, at 77 K, $K_2Cd_{2.7}Mn_{0.3}S_4$ emitted red light with a single maximum at 1.84 eV (671 nm) and only a shoulder was present at 1.78 eV; see Figure 10B. The 77 K excitation spectrum of $K_2Cd_{2.7}Mn_{0.3}S_4$ was detected at 1.84 eV (671 nm) and again revealed the presence of two bands. The first had a maximum at 3.31 eV (370 nm) and displayed a drop

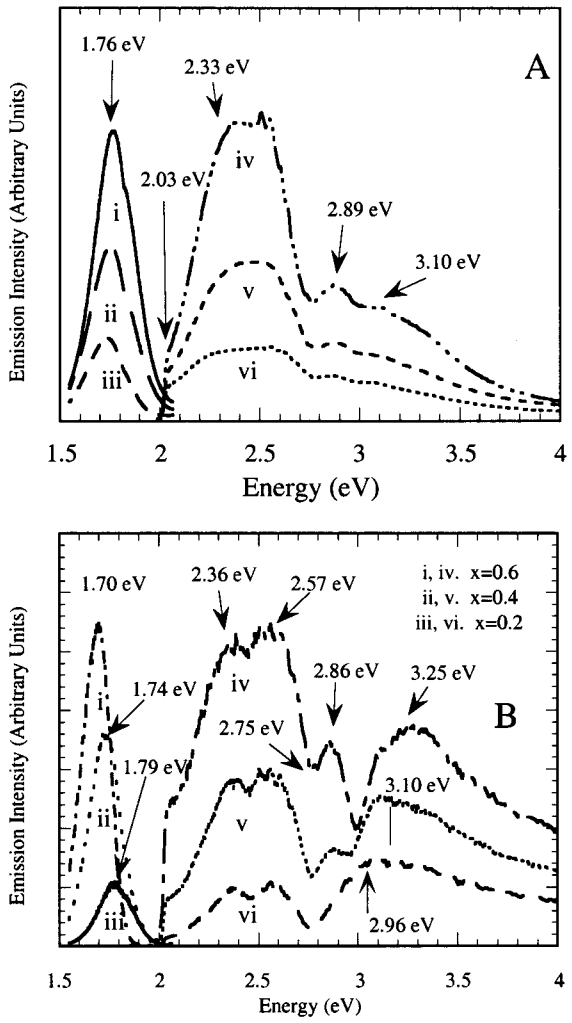

Figure 11. (A) Room-temperature photoluminescence spectra of $K_2Cd_{2.4}Mn_{0.6}S_4$, $K_2Cd_{1.8}Mn_{1.2}S_4$, and $K_2Cd_{1.2}Mn_{1.8}S_4$ ((i)−(iii) Emission, $E_{exc} = 2.33$ eV; (iv)−(vi) excitation, $E_{det} = 1.76$ eV). (B) 77 K photoluminescence spectra of $K_2Cd_{2.4}Mn_{0.6}S_4$, $K_2Cd_{1.8}Mn_{1.2}S_4$, and $K_2Cd_{1.2}Mn_{1.8}S_4$ ((i)−(iii) Emission, $E_{exc} = 2.57$ eV; (iv) excitation, $E_{det} = 1.70$ eV; (v) excitation, $E_{det} = 1.74$ eV; (vi) excitation, $E_{det} = 1.79$ eV).

in intensity from approximately 3.08 eV (403 nm) to 2.76 eV (449 nm). The lower energy band possessed a maximum at 2.36 eV and fell rapidly to a value of 2.11 eV (588 nm). An emission spectrum obtained at this lower energy maximum is qualitatively similar, though weaker than that obtained at 3.31 eV.

$K_2Cd_{2.4}Mn_{0.6}S_4$ ($x = 0.2$), $K_2Cd_{1.8}Mn_{1.2}S_4$ ($x = 0.4$), and $K_2Cd_{1.2}Mn_{1.8}S_4$ ($x = 0.6$). The room temperature photoluminescence spectra of these three compounds are similar with the major difference being intensity. Apparently, the optical characteristics introduced by the incorporation of manganese become fully developed at $x = 0.2$. Further increases in Mn content cause only minor changes in the optical properties.

With an exciting line of 2.33 eV (532 nm) these compounds showed intense red emission at room temperature with all maxima at 1.76 eV (705 nm); see Figure 11A. The room-temperature excitation spectra were detected at 1.76 eV (705 nm) and displayed maxima at 2.55 eV (486 nm). The bands remained rather flat to a value of 2.33 eV (532 nm), after which they fell rapidly to zero at approximately 2.03 eV (611 nm). This lower energy band agrees well with the value of the mid-gap feature in the absorption spectra and it is attributed to Mn levels. Higher energy features are observed at 2.89 eV (429 nm) and 3.10 eV (400 nm). Qualitatively, the intensity of light emission decreases with increasing Mn content, suggesting that high Mn concentration levels quench the room-temperature photoluminescence in these compounds.

Several differences exist between the room-temperature and 77 K spectra. At 77 K the compounds show red luminescence, but the maxima shift to lower energy with increasing Mn concentration; see Figure 11B. These maxima vary from 1.79 eV (693 nm) for the $x = 0.2$ sample to 1.74 eV (713 nm) for the $x = 0.4$ and 1.70 eV (729 nm) for the $x = 0.6$ samples, respectively. This behavior can be rationalized if light emission involves a Mn-based band which grows wider with increasing Mn content. A striking difference between the room-temperature data and the data at 77 K is that in the latter the intensity dependence on the Mn concentration is reversed, with the least intense spectra obtained from the $x = 0.2$ sample. The excitation spectra obtained at 77 K and detected at each respective emission maximum revealed a complicated pattern of peaks. Four maxima occur, at 3.25 eV (381 nm), 2.86 eV (434 nm), 2.57 eV (482 nm), and 2.36 eV (525 nm), for the $x = 0.6$ sample. With increasing Mn content, the maximum of the highest energy peak moves from 3.25 eV (381 nm) to 3.10 eV (400 nm); see Figure 11B.

$K_2Cd_{0.39}Mn_{2.61}S_4$ ($x = 0.87$). The luminescence properties of $K_2Cd_{0.39}Mn_{2.61}S_4$ are similar to those of materials with lower x values, even though there has been a structural change. With an exciting energy of 2.51 eV (494 nm), this compound showed intense red emission at room temperature with a maximum at 1.75 eV (709 nm); see Figure 12A. The room-temperature excitation spectrum of $K_2Cd_{0.39}Mn_{2.61}S_4$ was detected at 1.75 eV (709 nm) and displayed a maximum at 2.51 eV (494 nm) which fell rapidly to zero at approximately 2.04 eV (608 nm). Higher energy features were observed at 2.56 eV (484 nm), 2.61 eV (475 nm), 2.88 eV (431 nm), and 3.09 eV (401 nm).

At 77 K, the red luminescence of $K_2Cd_{0.39}Mn_{2.61}S_4$ shifts slightly with a maximum located at 1.69 eV (734 nm) when it was excited with 2.39 eV (519 nm) light; see Figure 12B. The 77 K excitation spectrum of $K_2Cd_{0.39}Mn_{2.61}S_4$, detected at 1.69 eV (734 nm), was similar in complexity to spectra obtained for the lower x value samples. The maximum value of the emission occurred at 2.39 eV (519 nm). Higher energy features occurred at 2.50 eV (496 nm), 2.86 eV (434 nm), 3.10 eV (400 nm), and 3.34 eV (371 nm). In a manner similar to the $x = 0.2$−0.6 samples, $K_2Cd_{0.39}Mn_{2.61}S_4$ revealed a sharp drop in intensity at 2.04 eV (608 nm).

Thermal Properties. Differential thermal analysis (DTA) of representative members of the $K_2Cd_{3(1-x)}Mn_{3x}S_4$ family ($x = 0.2$, 0.4, 0.6, and 0.87) showed that they melt congruently at 822, 839, 863, and 893 °C, respectively. In Figure 13, a representative DTA diagram for $K_2Cd_{3(1-x)}Mn_{3x}S_4$ ($x \sim 0.2$) is displayed, with the temperature and interpretation of each peak included. X-ray powder diffraction patterns indicated that no decomposition occurred after melting.

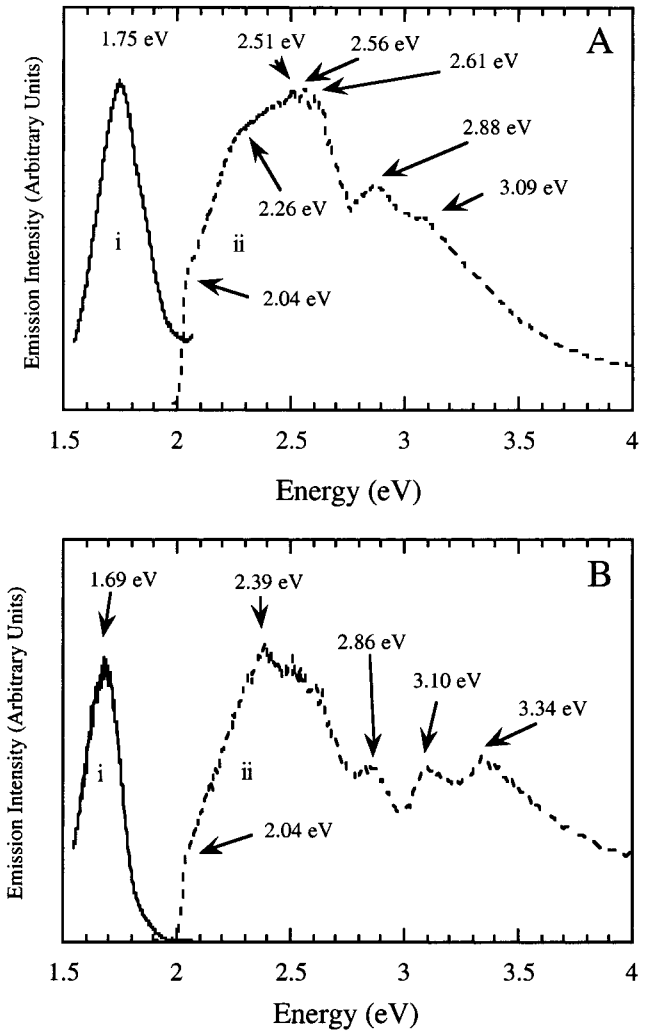

Figure 12. (A) Room-temperature photoluminescence spectra of $K_2Cd_{0.39}Mn_{2.61}S_4$ ((i) Emission, $E_{exc} = 2.51$ eV; (ii) excitation, $E_{det} = 1.75$ eV). (B) 77 K photoluminescence spectra of $K_2Cd_{0.39}Mn_{2.61}S_4$ ((i) Emission, $E_{exc} = 2.39$ eV; (ii) excitation, $E_{det} = 1.69$ eV).

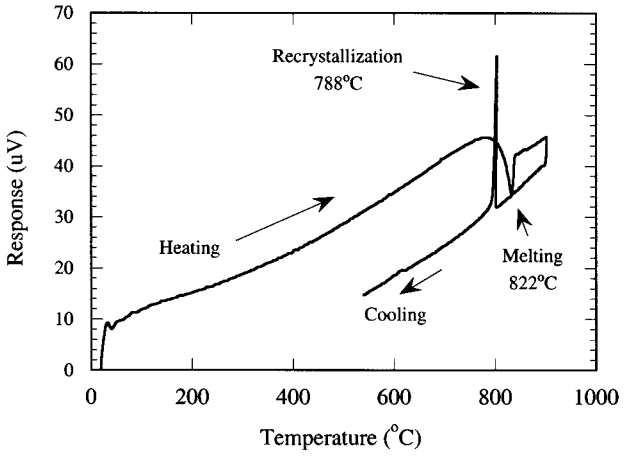

Figure 13. DTA diagram of $K_2Cd_{2.4}Mn_{0.6}S_4$. The melting and crystallization events are shown.

Magnetic Properties. In addition to the magnetic studies of $Cd_{1-x}Mn_xQ$ (Q = S, Se, Te)[3] solid solutions, other magnetically interesting chalcogenide systems have been investigated prior to this work. Bronger and co-workers explored the characteristics of $Cs_2Zn_{3(1-x)}Mn_{3x}S_4$ solid solutions.

Table 8. Magnetic Characteristics of the $K_2Cd_{3(1-x)}Mn_{3x}S_4$ Solid Solutions

composition	θ	C	M_{max} (emu/mol of Mn)	hysteresis	change in ZFC vs FC
$x = 0.05$	−14 K	0.7	5790	no	no
$x = 0.1$	−55 K	1.3	3915	no	no
$x = 0.2$	−112 K	2.0	1942	no	no
$x = 0.4$[a]	−222 K	3.5	839	slight	slight
$x = 0.6$	−597 K	7.0	362	yes	yes
$x = 0.87$	−1038 K	9.4	237	slight	yes
$x = 0.883$	−238 K	2.2	237	slight	yes

[a] Precisely at what value of x does the CW law quit being in effect is not known. In any case at approximately $x > 0.4$ the θ and C values essentially lose their intended meaning and are shown for comparison only.

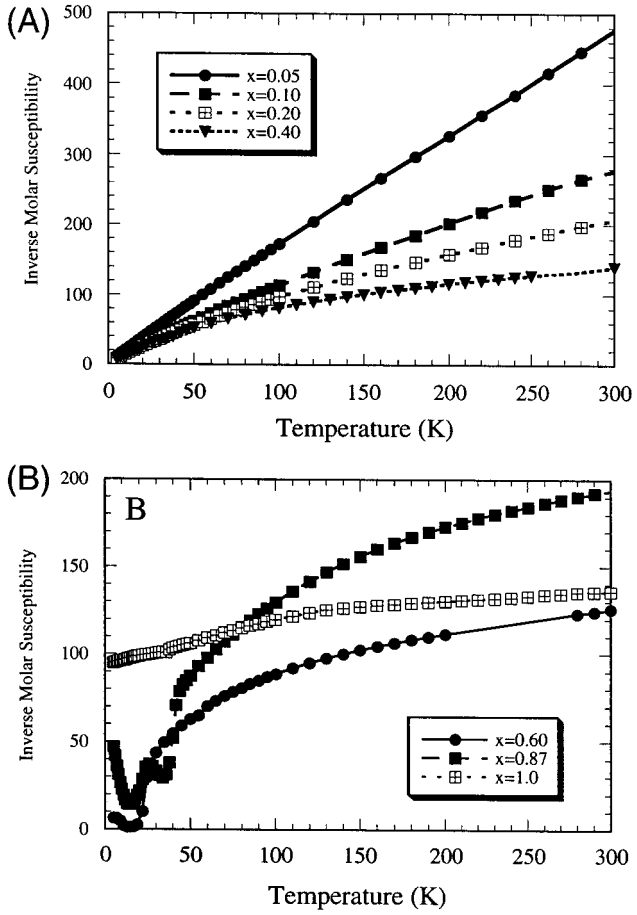

Figure 14. (A) Temperature-dependent, inverse molar susceptibility of $K_2Cd_{2.85}Mn_{0.15}S_4$ ($x = 0.05$), $K_2Cd_{2.7}Mn_{0.3}S_4$ ($x = 0.1$), $K_2Cd_{2.4}Mn_{0.6}S_4$ ($x = 0.2$), and $K_2Cd_{1.8}Mn_{1.2}S_4$ ($x = 0.4$). (B) Temperature-dependent, inverse molar susceptibility of $K_2Cd_{1.2}Mn_{1.8}S_4$ ($x = 0.6$), $K_2Cd_{0.39}Mn_{2.61}S_4$ ($x = 0.87$), and $K_2Mn_3S_4$ ($x = 1.0$).

$Mn_{3x}S_4$ and found antiferromagnetic ordering.[27] These materials crystallize in the $Cs_2Zn_3S_4$ structure with $(M_3Q_4)_n^{2n-}$ layers such as those described above in $K_2Cd_{0.35}Mn_{2.65}S_4$. The layers of the $Cs_2Zn_3S_4$-type structure adopt an ordered defect anti-PbO type. The defects are Zn vacancies from a hypothetical Zn_4S_4 anti-PbO lattice. These vacancies leave behind square holes in the form of M_4S_4 rings. The $(Zn_3S_4)_n^{2n-}$ layers possess even numbers of metal atoms in every M_4S_4 ring; thus, the magnetic moments may easily orient themselves in

(27) Bronger, W.; Hendriks, U.; Müller, P. *Z. Anorg. Allg. Chem.* **1988**, *559*, 95−105.

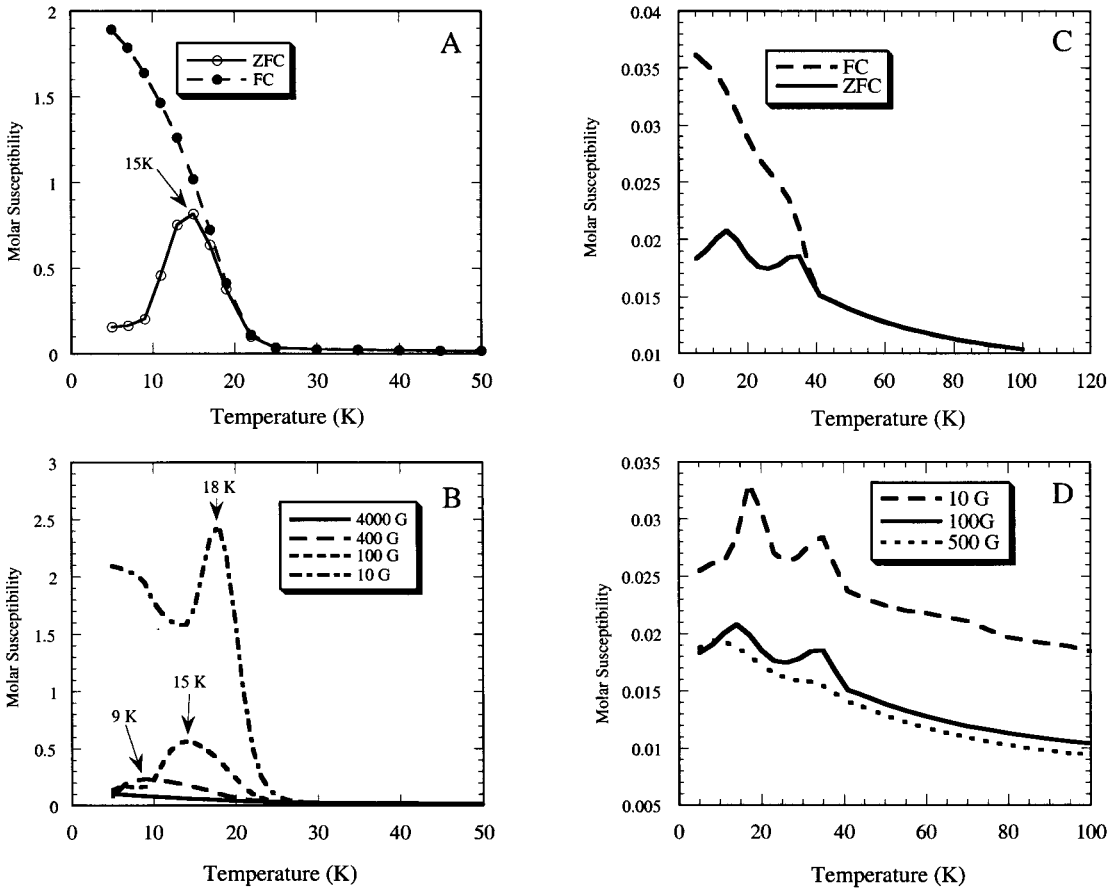

Figure 15. (A) Molar susceptibility versus temperature for $K_2Cd_{1.2}Mn_{1.8}S_4$ ($x = 0.6$) [$H = 100$ G]. (B) Molar susceptibility of the ZFC data versus temperature for $K_2Cd_{1.2}Mn_{1.8}S_4$ ($x = 0.6$) at various applied fields. (C) Molar susceptibility versus temperature for $K_2Cd_{0.39}Mn_{2.61}S_4$ ($x = 0.87$) [$H = 100$ G]. (D) Molar susceptibility of the ZFC data versus temperature for $K_2Cd_{0.39}Mn_{2.61}S_4$ ($x = 0.87$) at various applied fields.

an anti-ferromagnetic fashion. On the other hand, the $K_2Cd_3S_4$ structure type contains triangles with three metal atoms in a truncated cuboidal fragment, raising the possibility of frustrated spins. Therefore, a study of the magnetic behavior of the $K_2Cd_{3(1-x)}Mn_{3x}S_4$ solid solutions was deemed interesting because they represent a new host lattice.

None of the samples showed Curie−Weiss (CW) Law behavior for the full temperature range except for very low Mn content (e.g., <0.1). Despite this, the high-temperature data ($T > 100$ K) could be fit to CW Law. The values of θ and C as well as other magnetic characteristics are given in Table 8. For $x \leq 0.4$, the $1/\chi_{mol}$ plots obtained from the ZFC data show Weiss constants of −14, −55, −112, and −222 K for the $x =$ 0.05, 0.1, 0.2, and 0.4 samples, respectively; see Figure 14A. In this concentration range both C and θ do increase linearly with Mn content. The antiferromagnetic coupling observed becomes increasingly strong with increasing Mn content. The values of C also increase with increasing Mn content for the $x = 0.05$, 0.1, 0.2, and 0.4 samples, respectively, consistent with an increasing number of $S = {}^5/_2$ centers.

For the $x > 0.6$ samples, the values of C and θ obtained from the high-temperature data continue to increase; see Figure 14B. The increasing θ values indicate further increases in the strength of the antiferromagnetic coupling, as expected from the increasing concentration of Mn centers in the sample. However, given that it is questionable whether CW behavior is still in effect in these samples, any attempt to extract a C and θ is of limited value. The shape of the curve for the end member $K_2Mn_3S_4$ is very similar to that of $Cs_2Mn_3S_4$.[27,28]

As the concentration of Mn increases, the susceptibility deviates from CW behavior in ways that depend on the various Mn−S−Mn super-exchange interactions. At high Mn concentrations, one may expect a magnetic phase transition. Some possible transitions are from paramagnetic (P) behavior to a long-range ordered ferromagnetic (F), antiferromagnetic (AF), or ferrimagnetic (FI) state. Another possibility is a transition from P behavior to a short-range spin glass (SG) state. In a SG state, the spins are located randomly on structurally disordered sites so that the exchange interactions are "in conflict." At the freezing temperature, T_f, the spins freeze into what appear to be random directions but are in fact the result of the system attempting to resolve the conflict. A signature of the P to SG transition is a maximum in the χ_m vs. T curve measured when the sample is cooled in zero field (ZFC), with somewhat different behavior observed if the sample is cooled in a field (FC). Which of these phases actually occurs depends on the sign of the nearest neighbor and the next nearest neighbor exchange interactions as well as the disorder and subsequent competition between these

(28) $K_2Mn_3S_4$ appears to have complex magnetic behavior which includes a ferromagnetic transition at 44 K. The properties of this material are outside the scope of this paper. Hanko, J.; Kanatzidis, M. G., unpublished results.

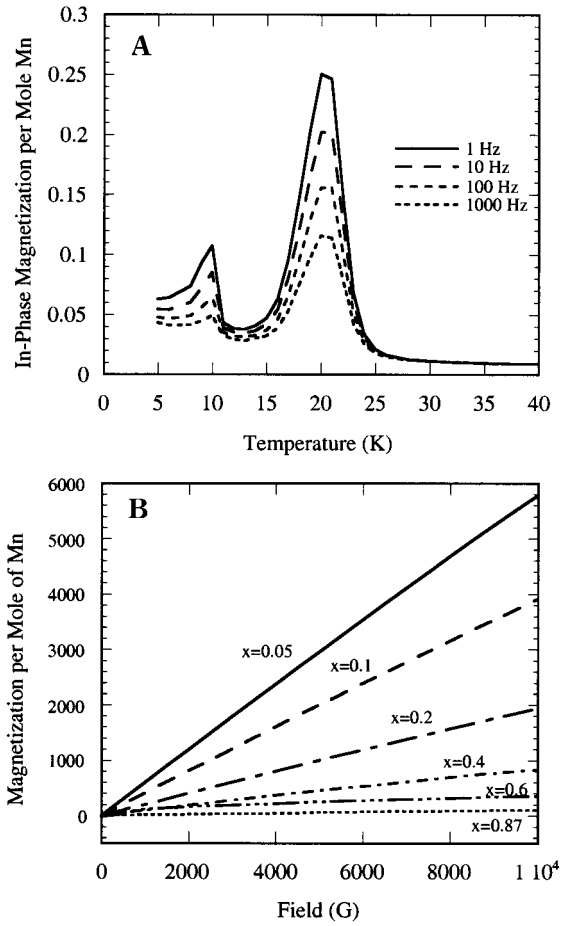

Figure 16. (A) Temperature-dependent, in-phase magnetization for $K_2Cd_{1.2}Mn_{1.8}S_4$ ($x = 0.6$) at various driving frequencies. (B) The field dependence of the magnetization for several $K_2Cd_{3(1-x)}Mn_{3x}S_4$ solid solutions (Inset: the low field region of the $x = 0.6$ sample).

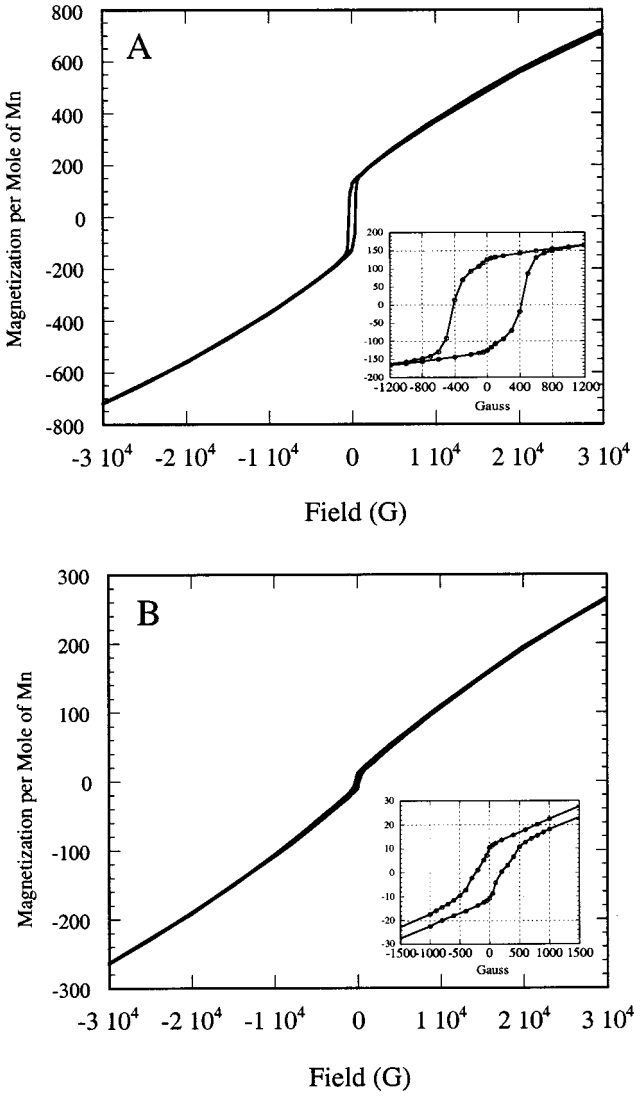

Figure 17. (A) Hysteresis behavior of $K_2Cd_{1.2}Mn_{1.8}S_4$ ($x = 0.6$). (B) Hysteresis behavior of $K_2Cd_{0.39}Mn_{2.61}S_4$ ($x = 0.87$).

interactions. (There exist so-called "re-entrant spin glass" systems that exhibit two successive phase transitions with decreasing temperature, a P to F transition followed by a SG transition).

It is at $x = 0.6$ that a transition to an ordered magnetic phase is first observed with differences between the ZFC data and the FC data, see Figure 15. This behavior is somewhat suggestive of spin glass behavior. In Figure 15A, the data were obtained with a measuring field of 100 G. The location of the peak in the ZFC data is dependent on the magnitude of the applied field for this composition; see Figure 15B. With increasing applied field, the peak broadens and becomes weaker. The temperatures of the peaks are 18, 15, and 9 K for the runs at 10, 100, and 400 G, respectively. At 4000 G, the peak is washed out or it occurs below 5 K. This behavior, too, is reminiscent of a spin glass where, with increasing field, one must go to lower temperatures to achieve freezing of the spins in random orientations.

The $x = 0.87$ phase also shows substantial differences between the ZFC data and the FC data. Two peaks are observed in the ZFC data, at 14 and 39 K; see Figure 15C. These data are consistent with spin-glass-like behavior as well; however, the existence of two peaks is puzzling. Possible reasons for the two peaks may be the presence of two different phases or the presence of crystals with two different concentrations of Mn (e.g., concentration gradients). None of these possibilities could be distinguished from the XRD powder patterns or microprobe EDS analyses of these samples. This behavior, however, may also be due to a single phase because it was reproducible from batch to batch. The locations of the two peaks are dependent on the applied field in this sample as well; see Figure 15D. The higher temperature peak has values of 35, 34, and 33 K for $H = 10$, 100, and 500 G, respectively. The lower temperature peak occurs at 17, 15, and 10 K for $H = 10$, 100, and 500 G, respectively.

The temperature-dependent ac magnetization was determined for the $x = 0.6$ and $x = 0.87$ samples.[29] The $x = 0.6$ sample showed two peaks, at 9 and 21 K, and no frequency dependence; see Figure 16. The in-phase and out-of-phase data sets contained peaks at the same temperatures, varying only in intensity. For $K_2Cd_{0.39}$-

(29) In an ac measurement, one observes both the in-phase and out-of-phase components of the magnetization. In P, F, AF, and FI systems, where there is no serious time dependence of the magnetization, and there are no interesting features in the ac magnetization. In SG systems, where the magnetization varies logarithmically with time, the peak in the magnetization versus temperature curve occurs at a freezing temperature, T_f, which decreases with increasing measuring time (reciprocal of the measuring frequency) approaching the true phase transition temperature T_{sg} in the limit of infinite measuring time.

$Mn_{2.61}S_4$ ($x = 0.87$), a much weaker response was observed. Two peaks, at 18 and 35 K, were observed with driving frequencies of 1 and 10 Hz. At 100 and 1000 Hz, the data sets were too noisy to be reliable. It is interesting to note that the peaks for the $x = 0.87$ material seem to agree with the two peaks in the dc data, as does the high-temperature peak in the $x = 0.6$ sample.

Hysteresis. To further assess any spin-glass-like behavior, we performed field-dependence measurements in field-cooled and zero-field-cooled samples. In a spin glass, the shape and position of the loop may depend on the field in which the sample was cooled prior to "cycling". For each composition, the field dependence at 5 K was determined. None of the samples appeared to reach a saturation field; see Figure 17A. The $x = 0.6$ sample, however, displayed an inflection point in the data; see the inset in Figure 17. The decreasing values of the magnetization with *increasing* Mn content suggest that at higher x values larger percentages of the manganese atoms are paired antiferromagnetically, consistent with the increasingly negative θ values. This could be due to the formation of antiferromagnetic dimers which "drop out" of the magnetization.

The hysteresis behavior was investigated for the $x = 0.4$, 0.6, and 0.87 samples. The 0.4 sample shows no hysteresis at all, while the 0.6 sample shows significant hysteresis; see Figure 17A. For the $x = 0.6$ sample, a remnant magnetization of 125 emu/mol Mn was observed at 0-G applied field, and a coercive field of 413 G. It is interesting to note that the hysteresis loop does not attain saturation up to 30 000 G and this could be a further indication of spin-glass behavior in this system.

The hysteresis behavior of $K_2Mn_{2.61}Cd_{0.39}S_4$ ($x = 0.87$) was much weaker than that of the $x = 0.6$ sample. The remnant magnetism is 4.3 emu/mol Mn, while the coercive force is 195 G; see Figure 17B. The shape of the hysteresis loop is also poor and the loop never really closes on itself because saturation is not achieved up to the highest available field. The smaller dimensions of the hysteresis loop compared to the $x = 0.6$ sample indicate both that a smaller number of spins remain aligned at zero field and that a smaller opposing field is necessary to reverse the spins. These effects could be due to the increase in the manganese content and/or the structural change in this sample.

The above magnetic data may indicate the presence of finite length chains (clusters) of manganese atoms, running in a zigzag manner through the layers. The chains are expected to possess antiferromagnetic coupling between manganese atoms.[30] The end members of odd numbered chains however may contribute to paramagnetic behavior. With increasing amounts of manganese, the chains lengthen, increasing the amount of antiferromagnetic behavior and decreasing the number of lone paramagnetic manganese atoms. What remains to be discerned is how these chains interact with each other to produce the ordering observed in the temperature dependence and hysteresis data. Chains of metal atoms in the same layer, spaced by a cadmium atom, could interact ferromagnetically. These interactions are expected to be weak because they are next nearest neighbor interactions. Between layers metal atoms are connected by a M−S−K−S−M sequence. The exchange is expected to be weak here, too, because the K−S bonds are long and possess high ionic character. A theoretical calculation of the magnetic susceptibility for the $K_2Cd_{3(1-x)}Mn_{3x}S_4$ solid solutions will be complicated both by the highly anisotropic nature of these layered materials and the complicated exchange geometry within each layer. Although we have pointed out that at high x values the magnetic properties are "spin-glass-like", we cannot confidently state that they are in fact spin glasses because they do not possess all the attributes associated with such behavior (e.g., lack of ac frequency dependence, etc.). It is possible that some of these observations may also partially fit the description for canted antiferromagnetism. Additional work is needed to further clarify this issue.

Concluding Remarks

A series of congruently melting $K_2Cd_{3(1-x)}Mn_{3x}S_4$ solid solutions has been demonstrated. These are magnetic semiconductors which are chemically derived from CdS but with larger energy band gaps than those of the binary sulfide. For $x < 0.6$, these solid solutions feature $(M_3S_4)_n^{2n-}$ layers assembled only of truncated $(M_3S_4)^{2-}$ cubes. A phase change and a structural reorganization of the layers occurs between $0.6 < x < 0.9$. The new layers are similar to those found in $Cs_2Zn_3S_4$. At $x = 1$ the structure changes again, though it remains layered, to the $K_2Mn_3S_4$ type. The compounds display red emission, even at room temperature, which suggests possible applications as red phosphors. The emission intensity and type depends strongly on x. Small amounts of Mn cause a small bathochromic shift in the emission, but increasing amounts quench the photoluminescence. This is reminiscent of a previous study in which the dependence of luminescence intensity on manganese-ion concentration in the dilute magnetic semiconductors $Cd_{1-x}Mn_xTe$ with $0.4 < x < 0.7$[31] was shown to saturate because of effective nonlinear quenching already at low excitation levels. The unique, layered structure of the parent compound $K_2Cd_3S_4$ provides an interesting host lattice for the insertion of magnetic centers such as manganese. The magnetic behavior of these solid solutions is unusual and does not fit well any of the standard magnetism models. Although antiferromagnetic coupling is observed in most cases, with very high Mn content and at low temperatures, transitions to magnetically complex phases are observed. Other divalent magnetic centers such as Co and Fe should also give analogous solid solutions.

Acknowledgment. This research was made possible with funding from NSF Grant DMR-9817287. This work made use of a scanning electron microscope located in the Center for Advanced Microscopy at Michigan State University.

Supporting Information Available: Crystal data and anisotropic thermal parameters for $K_2Mn_3S_4$ and $K_2Cd_{0.35}Mn_{2.65}S_4$ (PDF). This material is available free of charge via the Internet at http://pubs.acs.org.

CM0100422

(30) Bronger, W.; Muller, P. *J. Alloy Compds.* **1997**, *246* (1−2), 27−36.

(31) Agekyan, V. F.; Vasil'ev, N. N.; Serov, A. Y. *Phys. Solid State* **1999**, *41*, 41−44.